UNIVERSITY OF BIRMINGHAM

Experimental and computational examination of protein-surface interactions

Mallinson, David; Cheung, David; Simionesie, Dorin; Mullen, Alexander ; Zhang, Zhenyu; Lamprou, Dimitrios

Document Version
Peer reviewed version

[Link to publication on Research at Birmingham portal](#)

Experimental and computational examination of protein-surface interactions

Journal:	*Journal of Biomedical Materials Research: Part A*
Manuscript ID	Draft
Wiley - Manuscript type:	Original Article
Date Submitted by the Author:	n/a
Complete List of Authors:	Mallinson, David; University of Strathclyde, Strathclyde Institute of Pharmacy and Biomedical Sciences Cheung, David; National University of Ireland, School of Chemistry Simionesie, Dorin ; University of Birmingham, School of Chemical Engineering Mullen, Alexander; University of Strathclyde, Strathclyde Institute of Pharmacy and Biomedical Sciences Zhang , Zhenyu Jason; University of Birmingham, School of Chemical Engineering Lamprou, Dimitrios; University of Strathclyde, Strathclyde Institute of Pharmacy and Biomedical Sciences
Keywords:	Atomic force microscopy, molecular dynamics, polyurethane, poly (methyl methacrylate), fibronectin

SCHOLARONE™
Manuscripts

Experimental and computational examination of protein-surface interactions

David Mallinson[1], David L. Cheung[2*], Dorin Simionesie[3], Alexander B. Mullen[1], Zhenyu J. Zhang[3*], Dimitrios A. Lamprou[1,4*]

[1]Strathclyde Institute of Pharmacy and Biomedical Sciences (SIPBS), University of Strathclyde, 161 Cathedral Street, Glasgow, United Kingdom.

[2]School of Chemistry, National University of Ireland, Galway, University Road, Galway, Ireland.

[3]School of Chemical Engineering, University of Birmingham, Edgbaston, Birmingham, United Kingdom.

[4]EPSRC Centre for Innovative Manufacturing in Continuous Manufacturing and Crystallisation (CMAC), University of Strathclyde, Glasgow, United Kingdom.

*Corresponding Authors. E-mails: david.cheung@nuigalway.ie, z.j.zhang@bham.ac.uk, dimitrios.lamprou@strath.ac.uk, Tel.: +44(0)1415484968

Keywords: Atomic force microscopy, molecular dynamics, polyurethane, poly (methyl methacrylate), fibronectin.

Abstract: Using a combination of experimental and computational approaches, the interaction between anastellin, a recombinant fragment of fibronectin, and representative biomaterial surfaces has been examined. The molecular interaction was directly quantified by atomic force microscope (AFM) based force spectroscopy, complemented by adsorption

1

Journal of Biomedical Materials Research Part A

measurements using quartz crystal microbalance (QCM). It was found that the anastellin molecules facilitates a stronger adhesion on polyurethane films (72.0 pN nm^{-1}) than on poly (methyl methacrylate) films (68.6 pN nm^{-1}). This is consistent with the adsorption measurements of anastellin on the two polymeric surfaces, observed by QCM. Molecular dynamics simulations of the behaviour of anastellin on polyurethane in water solution were performed to rationalise the experimental data, and show that anastellin is capable of rapid adsorption to PU while its secondary structure is stable upon adsorption in water.

INTRODUCTION

In order to design medical devices that are exposed to physiological environments with prolonged service life and enhanced biocompatibility, it is vital to understand how biological objects interact with the surface of the engineered component, and the underlying biophysical mechanisms. For the development of biomaterials, the predominant mechanisms include the adsorption of proteins which is the initial stage for cell adhesion. [1] One of the major proteins that significantly affects the compatibility of biomaterials used intracorporeally is fibronectin (Fn). This is an important extracellular protein that exists in a variety of forms (e.g. circulating plasma, tissue and cellular). [2] It is made up of three types of domain (I, II and III). Types I and II are stabilised with disulphide bonds while type III fibronectin domains (FnIII) are capable of unfolding under tension. This can expose hidden, cryptic binding sites such as the Arg-Gly-Asp (RGD) sequence found in the tenth fibronectin type III domain (FnIII10) and the Pro-His-Ser-Arg-Asn (PHSRN) sequence in the ninth fibronectin type III domain (FnIII9). The RGD sequence allows binding to cell-bound integrin receptors, such as α5β1, to enable adhesion of cells to the extracellular matrix while the PHSRN sequence has a synergistic effect on this binding. [3] The RGD peptide sequence has been incorporated onto

2

Journal of Biomedical Materials Research Part A

biomaterials, [4-6] in its linear form, or cyclic forms, or as part of a larger fragment in order to improve aspects of biocompatibility such as osseointegration. [4] Use of a protein fragment offers advantages over whole Fn such as improved stability and increased density of desired sequences on the surface. [7]

Another area of Fn that has been shown to elicit potentially useful interactions is the C-terminal fragment of the first FnIII domain (FnIII1c), known as anastellin, which has 76 amino acid residues. [8-12] The FnIII1 domain has been identified as a region associated with matrix formation by Fn-Fn interactions. [13] When mixed with whole Fn molecules, anastellin can create a different form of Fn known as superfibronectin which is adept at supporting cell adhesion and spreading. [10,14] Anastellin and superfibronectin have been reported to contribute towards anti-tumour, anti-metastatic, and anti-angiogenic performance through a mechanism that involves extracellular signal-regulated kinases (ERK) and a decrease in cyclin D1, cyclin Al, and cyclin-dependent kinase 4 (cdk4). [9,15-18]

Upon adsorption to solid surfaces, the conformation of Fn at the interface appears to depend largely on the characteristics of the surface. Proteins tend to adopt an extended conformation on hydrophilic surface but a compact, globular conformation on hydrophobic surfaces. [19,20] Furthermore, other factors such as surface chemistry and topography have been found to play an important role. [21,22] Hydrophobic surfaces adsorb more Fn than hydrophilic surfaces, [19] the globular conformation adapted could accommodate more molecules and hence a greater packing density. [23] The change of conformation to an elongated form is important since it can expose the aforementioned binding sites such as RGD and PHSRN and allow matrix formation and cell attachment. Interaction between protein and solid surface and the consequent confirmation can be examined with a wide range of experimental approaches including atomic force microscopy (AFM), quartz crystal microbalance, fluorescence

3

Journal of Biomedical Materials Research Part A

resonance energy transfer (FRET), measuring the adsorption amount of labelled Fn, and enzyme-linked immunosorbent assays (ELISA). [19,20,24,25]

With the readily controlled molecular structure, chain length, and functional groups, polymers have been widely used as biomaterials. Examples include polyurethane (PU) for ureteral catheters, [26] poly (methyl methacrylate) (PMMA) as bone cement, [27] polytetrafluoroethylene (PTFE) as artificial heart valves and vascular grafts, [28] and ultra-high density polyethylene in joint replacement implants. Palacio *et al.* [29,30] have investigated the adhesion of whole Fn, bovine serum albumin and collagen to PMMA surfaces as well as di- and triblock copolymers of PMMA with poly (2-hydroxyethyl methacrylate) (PHEMA) and/or poly (acrylic acid) (PAA). They used AFM in force-volume mode with probes coated with silane and protein, and reported that the PMMA regions of the polymer had lower adhesion than PAA regions due to weaker interactions between the polymer and hydrophobic regions of Fn. The adhesive force between Fn and PMMA was reduced from 1.0 nN to 0.7 nN as the pH of the surrounding medium is decreased from 7.4 to 6.2. It is possible that the protein is less negatively charged at lower pH so that the electrostatic repulsion from the acid groups of the polymer is reduced. Hydrophobicity ought to be an indicator of adhesion since it would affect the repulsive force between the protein and the polymer.

For a number of years, a molecular simulation approach has been used to investigate protein-surface adsorption, [31] giving significant insight into the mechanism of adsorption and the factors that drive this. Due to its relevance to biomaterials [1] the adsorption of a number of fibronectin modules onto surfaces have been investigated. [32-34] These have shown that fibronectin adsorption is relatively non-specific, with it readily adsorbing onto organic, [33] inorganic, [34] and graphite surfaces. [32]

4

Journal of Biomedical Materials Research Part A

In the present work, adhesion and adsorption of anastellin on to two polymeric films, PMMA and PU, were measured by AFM and QCM. Influences of both chemical composition and hydrophobicity of the polymeric surfaces on the protein-surface interaction were examined. The experimental results were then compared with the results of molecular dynamics simulations.

MATERIALS AND METHODS

Materials

Poly (methyl methacrylate) (PMMA; MW 94,600) was purchased from Acros Organics. Polyurethane (PU) was purchased from Fluka. The FnIII1c protein fragment, phosphate buffered saline (PBS; pH 7.4) tablets, tetrahydrofuran (THF; $\geq$ 99.9 %), ethylene glycol (EG; 99.8 %), diiodomethane (DIM; 99 %) and ethanol ($\geq$ 99.8 %) were purchased from Sigma.

Spin Coating

Silica wafer (SW) was cleaned with deionised water, followed by 70 % ethanol and finally with THF in order to sterilise the surface and remove both water-soluble and organic contaminants. Polymers were dissolved in THF (2 % w/v). Consequently, the polymer solution was spin coated onto silica wafer at 2,000 rpm for 30 s with a Laurell WS-400-6NPP spin coater as per Mallinson *et al.* [35]

Contact Angle Goniometry

The advancing contact angles (θ_A) of three solvents (deionised water (DW), ethylene glycol (EG) and diiodomethane (DIM)) on the two polymer surfaces were measured in order to calculate the surface energy (γ_s) and surface energy components of the surfaces. As per Mallinson *et al.* [35] small drops of DW (18.2 MΩ; surface tension (γ_L) 72.8 mN m^{-1} at 20 °C),

5

Journal of Biomedical Materials Research Part A

EG (γ_L 48.0 mN m^{-1} at 20 °C) and DIM (γ_L 50.8 mN m^{-1} at 20 °C) were placed on the surface with a needle, followed by measuring both the left and right contact angles with a Krüss DSA30B contact angle goniometer (CAG). At least 2 repeats were made for each surface with 3 drops per sample, resulting in at least 12 measurements per sample. Using these contact angle values, the surface energies were calculated using a Visual Basic application developed by Lamprou *et al*, [36] based on the formula proposed by Good and Oss. [37]

Circular Dichroism

Circular dichroism (CD) was performed in order to determine whether the protein fragment retained the expected structure when reconstituted. The protein sample was dissolved in PBS solution (pH 7.4) at 200 µg mL^{-1}. Spectra were read with a Chirascan CD spectrophotometer (Applied Photophysics) in the wavelength range 190-280 nm, with step size of 1 nm and bandwidth of 1 nm, using a quartz cuvette with a path length of 0.1 mm (Hellma). Three spectra were averaged and data were processed with Chirascan Viewer and with Microsoft Excel.

Atomic force microscopy

AFM measurements were performed in ambient using a Bruker Multimode 8 AFM equipped with a Nanoscope Controller V and SNL-10 probes (cantilever C: nominal spring constant 0.24 N m^{-1} and nominal resonant frequency 56 kHz). Cantilevers were silanised to allow protein functionalisation by submerging in 2 mM APTES in toluene for 5 min as per Couston *et al*. [38] The cantilevers were subsequently washed with toluene and deionised water in order to remove unbound silane. The FnIII1c protein fragment was added by incubating the tip in a drop of 1 mg mL^{-1} protein solution (in PBS pH 7.4) for 10 min followed by a thorough rinsing with deionised water to remove unbound protein. Each polymer surface was scanned 4 times with each AFM probe before and after protein functionalisation. This was done with

6

Journal of Biomedical Materials Research Part A

two different probes. For each of the AFM images approximately 160 curves were chosen at random from each of the force-volume images (20 curves x 4 areas x 2 probes). Deflection sensitivity was calibrated with a sapphire reference sample and the tip radius was determined with a PA01 spiked reference sample (Mikromasch). Ramps were made over 1×1 μm squares.

Surface roughness was determined using images captured using unfunctionalised probes in PeakForce-Quantitative Nanomechanical (PF-QNM) mode. Images were analysed with Bruker Nanoscope Analysis version 1.5 to view force curves and calculate surface roughness. Adhesion values were extracted from the ramps using an in-house Python script. Adhesive forces were then normalised for the effect of tip radius by dividing by tip radius in accordance with equation 1 by Sugawara *et al*. [39]

$A = 4\pi RT$ (Eq.1)

where A is the corrected adhesion, R is tip radius and T is surface tension of the medium.

Quartz Crystal Microbalance

Quartz crystal microbalance (QCM) is a technique that uses a mass sensor [40-42] to measure the adsorption of biopolymers [43,44] or synthetic electrolytes [45] from liquid and allows observation of not only the adsorption kinetics and adsorbed mass but also of the viscoelastic properties of adsorbed polymer layers at the solid liquid interface. [23,46,47] The technique relies upon the resonant frequency of a quartz crystal. A frequency shift (Δf) will be induced by any change in adsorbed mass, as Δf is related to the adsorbed mass per unit surface Δm, by a linear relationship known as the Sauerbrey equation (Eq. 2).

$$\Delta m = \frac{c\,\Delta f}{n}$$ (Eq. 2)

7

Journal of Biomedical Materials Research Part A

where n is the overtone number ($n = 1$ in the present case) and C is a constant that describes the sensitivity of the device the changes in mass. Additionally, the exponential decay of the oscillation amplitude, D, is recorded which can reveal information about the viscoelastic properties of the adsorbed layer.

PU and PMMA thin films were formed on gold coated AT-cut quartz crystals by spin-coating, by the same protocol as on the Si wafers, and a SiO_2 crystal was used to replicate the silica wafer surface. All crystals were purchased from Testbourne Ltd. The crystals were placed in a home-built quartz crystal microbalance and all measurement were taken at room temperature. For adsorption measurements, the QCM chamber was flooded with HPLC-grade water solution and left until the frequency stabilises to an equilibrium state at the liquid/solid interface may be achieved. The protein fragment was initially dissolved in PBS buffer (pH 7.4) with a concentration of 1.0 mg mL^{-1}, and further diluted by HPLC-grade water to a concentration of 0.025 mg mL^{-1}. The HPLC-water in the QCM chamber was then replaced by the protein solution while the change in frequency and dissipation was recorded. A representative QCM adsorption result is presented in Fig. 1 where changes in frequency and corresponding adsorbed amount are shown.

Fig. 1 Second axis graphs with frequency and mass.

Molecular dynamics

The simulated system consisted of a single anastellin molecule, a slab of PU, water and ions. The PU surface was constructed from slab of crystalline PU, consisting of 48 chains (three layers of sixteen), with each chain containing two monomer units. The slab was constructed

Journal of Biomedical Materials Research Part A

using the crystal structure for the *trans-trans*-dicyclohexylmethane 4,4'-diisocynate (HMDI) monomer determined by Nigar *et al.* [48] An energy minimisation followed by short (20 ps) NVT and NpT simulations of the slab in contact with a vacuum were performed. The remainder of the simulation box was filled with water and an energy minimization and short NVT run were performed on the resulting system. The structure of the surface was then held fixed for the remainder of the simulations.

The structure of anastellin was taken from RCSB (accession code: 1Q38). Initially the protein centre-of-mass is placed at $z = 40$ Å, approximately 20 Å from the PU surface. Four different initial orientations were used: Arg-down where the cluster of arginine residues was orientated towards the surface; Arg-up where the cluster of arginine residues orientated away from the surface; N-down where the N-terminus pointed towards the surface and C-down where the C-terminus pointed towards the surface. Cl^- and Na^+ ions are added to neutralise the +5e charge on the protein and simulate different salt conditions. The system is periodic in the x and y directions and has repulsive Lennard-Jones walls in the z-direction.

The protein was modelled using the Charmm27 force field (with CMAP corrections), [49] the Charmm Generalised Force Field [50] was used to model the PU surface, and water was modelled using the Charmm-variant of TIP3P water (with van der Waals interaction sites on the hydrogen atoms). All simulations were performed at 298 K, with the velocity rescaling algorithm of Bussi *et al.* [51] used to control the temperature. For each starting orientation and salt concentration simulations of 100 ns were performed, with a timestep of 2 fs. Bonds involving hydrogen atoms were constrained using the LINCS algorithm [52] and the water geometry was held fixed using the SETTLE algorithm. [53] Long-range electrostatics were modelled using particle-mesh Ewald summation [54] with a real space cut-off of 10 Å and a reciprocal space grid spacing of 0.16 Å^{-1}. Van der Waals interactions were truncated at 10 Å.

9

Journal of Biomedical Materials Research Part A

The simulations were performed using the Gromacs MD package, version 4.6.3. [55] Standard Gromacs tools were used to set up and analyse the simulations.

Statistical Analysis

Statistical analysis was performed in Microsoft Excel, Python and Minitab 17. A significance level of 5 % was chosen. Significance between adhesive forces under different conditions were determined with a one-way ANOVA with a Tukey test.

RESULTS AND DISCUSSION

Contact Angle Goniometry and Surface Energies

The contact angles of water on all substrates used are presented in Table 1 and agree well with the literature values for PMMA (74 ° [56] and 69 ° [29]), PU (85.1 ° [35]) and silica wafer (57.9 ° [35]). From the chemical structures of PU and PMMA, it can be estimated that PMMA would be more hydrophobic since displays a greater frequency of lone electron pairs. The surface energies and surface energy components for all the surfaces are shown in Table 2. The R_a values (Table 2), based on the surface topography images collected with AFM, show that the films are smooth − 2.0 ± 0.1 nm and 3.1 ± 0.3 nm for PMMA and PU respectively. This suggests that the adsorption of Fn [57] and water contact angle [35] are not affected by surface roughness.

Table 1 Advancing contact angles of SW, PMMA and PU surfaces, n = 12.

Table 2 Surface energy components by CAG and surface roughness by AFM of SW, PMMA, and PU surfaces.

10

Journal of Biomedical Materials Research Part A

Circular Dichroism

The negative maximum at 218 nm (Fig. 2) suggests anti-parallel beta sheets [58] as is expected

for the protein fragment in its native conformation as imaged by Briknarova et al [59] with

NMR spectroscopy.

Fig. 2 Circular dichroism (CD) spectrum of FnIII1c.

Atomic Force Microscopy

Anastellin functionalisation increases adhesion on all surfaces tested (Fig. 3). This may be

partly due to the protein functionalisation process possibly adding a small layer of crystals

from the PBS as well as the intended protein fragment. Such increases in tip radius do not

appear to be the only factor since the differences between the PMMA (16.8 % increase) and

PU (12.5 % increase) values are greater than those between the silica values (48.2 %

increase). Since tip radius is accounted for, the difference between the polymers and the

APTES-functionalised and protein-ATPES-functionalised probes is likely due to hydrophilic-

hydrophobic interactions between protein fragment and elements of the polymer chains as

found by Palacio *et al*. with the interactions between Fn and PMMA and poly (acrylic acid)

(PAA). [29] It appears that the adhesion of the anastellin-functionalised probes to the PU films

was greater than to PMMA films (data not shown), contrary to previous work. This could be

at least partly due to the fact that while Palacio *et al*.'s [29] experiments were performed under

liquid these were performed in air at ambient humidity reducing the role of hydrophilic-

hydrophobic interactions.

11

Journal of Biomedical Materials Research Part A

Fig. 3 Difference in adhesion force by surface between silanised probes (APTES) and protein-functionalised probes (anastellin). All differences are significant.

Quartz crystal microbalance

Fig. 4 Density of anastellin on SiO_2, PU and PMMA surfaces.

Fig. 4a shows a representative measurement of protein adsorption on PMMA, in which both frequency and the corresponding mass change are presented as a function of time. It is clear that upon the introduction of protein solution, the mass at the already equilibrated polymer-buffer solution interface is increased, which confirms the adsorption of protein on the polymeric film. And the adsorption amounts of the protein (the changed frequency) on three different surfaces are compared in Fig. 4b. It was found that protein adsorbed the most on the silica surface, which is consistent with the AFM measurements where strong adhesion between protein and silica surface was observed. The PU surface shows a higher adsorption than the PMMA albeit the relative broad error bar, which agrees with the adhesion results. The increase in experimental error between silica and the polymer coated surfaces can be attributed to the increased surface roughness on the polymer thin films present as proven in the contact angle experiments.

Journal of Biomedical Materials Research Part A

Molecular dynamics

The adsorption mechanism and adhesion of anastellin to the polymer surfaces required further investigation by molecular dynamics. Due to high adhesion in the AFM studies and high adsorption in the QCM studies PU was selected for these further studies.

Independent of starting orientation the protein adsorbs onto PU surface within 100 ns, however, the equilibrium protein-surface separation and orientation depend on the initial configuration (Fig. 5). Starting from the Arg-down configuration the protein adsorbs rapidly onto the surface with little change in the orientation (the protein lies parallel to the surface across the entire simulation). In this case the final protein centre of mass position is ~32 Å, which is comparable to the width of the PU layer plus half the protein width. For the other starting configurations, adsorption typically takes longer and often involves transient contacts between the surface and protein before permanent adsorption. Additionally, the final separation between the protein centre-of-mass and surface is substantially larger, suggesting that in these cases the bulk of the protein lies further from the surface. This can be seen through the protein orientation. In particular, when starting from the Arg-up configuration the protein reorients so the N-terminus is towards the surface, so the final orientation of the protein in this case is close to that found form starting in the N-down conformation. For the C-down starting conformation, for most of the simulation the protein lies normal to the surface with the C-terminus pointing down (θ ~180 °) but slow reorientations of the protein are evident, notably towards the end of the simulation.

Fig. 5 Protein centre-of-mass position (top) and orientation (bottom) for no salt simulations. Simulations starting in the Arg-down, Arg-up, C-down, and N-down conformations are denoted by black, red, green, and blue lines respectively.

Journal of Biomedical Materials Research Part A

Fig. 6 Simulation snapshots showing adsorption of anastellin on to polyurethane surface. (a) Protein in Arg-down starting configuration at (left to right) t = 0 ns, 13 ns, 25 ns, 47 ns, 50 ns, and 100 ns. (b) Protein in Arg-up starting configuration at (left to right) t = 0 ns, 5 ns, 10 ns, 48 ns, 55 ns, and 100 ns. (c) Protein in N-down starting configuration at (left to right) t = 0 ns, 1 ns, 15 ns, 20 ns, 50 ns, and 100 ns. (d) Protein in C-down starting configuration at (left to right) t = 0 ns, 1 ns, 10 ns, 27.5 ns, 47 ns, and 100 ns. Residues involved in adsorption (see text) are highlighted.

Qualitative information on protein adsorption may be found from viewing simulation snapshots. For the Arg-down conformation (Fig. 6), these show the rapid adsorption of the protein onto the PU surface, with little subsequent change to either the protein structure or orientation. From the Arg-up conformation, the protein initially reorients itself in solution so that the N-terminus is directed towards the surface (t = 5 ns), followed by attachment to the surface through this region. While adsorbed on the surface, the protein can slowly reorient. Similarly, when the protein is initially placed in the N-down conformation, the protein's N-terminus rapidly adsorbs onto the surface (t = 1 ns). For the C-down conformation the protein attaches through the C-terminus (t = 10 ns) but more slowly than for N-down conformation (whereas the N-down conformation attached to the surface after only 1 ns the C-down conformation is still in bulk water at this time). Compared to the N-down conformation the protein appears to have greater orientational freedom, which may also be seen from the variation in protein angle over time. While the initial attachment is through the residues at the extreme end of the C-terminus, this changes towards the end of the simulation, with residues at the C-terminus end of the beta-sheet coming into contact with the surface.

14

Journal of Biomedical Materials Research Part A

Fig. 7 Residue centre-of-mass positions for protein starting in (top to bottom) Arg-down, Arg-up, C-down, and N-down conformations.

The different starting orientations lead to attachment through different regions of the protein. This may be seen through considering the centre-of-mass positions of the individual residues (Fig. 7). Apart from the Arg-down conformation, in which most of the residues lie close to the surface, only small numbers of residues are typically in contact with the surface. For both Arg-up and N-down these are the N-terminus and the loop joining the third and fourth beta-strands (around residue 61). This second region contains a number of residues with hydrophilic side-chains, which are capable of forming hydrogen bonds with the polar groups in the PU surface. For the C-down orientation while the initial contact is through the C-terminal end at the end of the simulation this has detached from the surface with a loop containing residues 22 to 26 (joining the first and second beta-strands). Again this is a predominately hydrophilic region, which is consistent with the highest adsorption being found for hydrophilic surfaces. The residues that are in contact with the surface (taken to be those with separation between the surface and centres-of-mass less than 5 Å) are shown in Table 3.

Table 3 Residues in contact with surface

Fig. 8 (a) Secondary structure amounts for (top to bottom) Arg-down, Arg-up, C-down, and N-down starting conformations. Black, red, and green lines denote turn, beta-strand, and random coil respectively. (b) Secondary structure distributions for (top to bottom) Arg-down, Arg-up, C-down, and N-down starting conformations.

15

Journal of Biomedical Materials Research Part A

Surface adsorption has little effect on the structure of the protein. Shown in Fig. 8a are the secondary structure compositions for the different starting structures. In all cases the structure remains predominately beta-strand, with turn and random coil. Apart from N-down, there is a slight increase in the amount of random coil when the protein adsorbs, with the amount of turn decreasing. For N-down the amount of random coil and turn remains largely unchanged across the simulation, in agreement with the CD measurements. The distribution of the different secondary structure motifs is also largely unchanged during the simulations (Fig. 8b).

From consideration of all of the simulations it may be seen that three particular regions of the protein are especially important in mediating attachment; these are the loop joining the first and second beta-strands (around residue 23), the loop joining the third and fourth beta-strands, and the C-terminus. These contain predominately hydrophilic residues, with attachment being driven by hydrogen bonding between these groups and the N-H and C=O groups in the PU. Adsorption through flexible regions suggests that these play a role in mediating surface adsorption, similar to the fly-casting mechanism exhibited by some DNA-binding proteins. [60]

The use of silanisation to functionalise the AFM probe means that the protein attaches to the probe via the N-terminal [61] since this allows covalent bonding. Protein that is not covalently bonded to the AFM probe ought to be removed by the washing stages. This method for protein functionalisation has been used previously for antibodies [38] and for Fn. Attachment of protein by the N-terminal would suggest that the C-down, Arg-down and Arg-up orientations used in the MD simulations are most relevant to the situation in the AFM experiments while all orientations are relevant to the QCM experiments.

16

Journal of Biomedical Materials Research Part A

CONCLUSION

In this paper the adsorption of anastellin, a C-terminal fragment of the fibronectin type III domain, onto biomaterial surfaces was investigated using a combination of experimental and theoretical methods. Understanding the adsorption of proteins onto synthetic surfaces is of interest in the development of new materials for medical applications. By combining a number of different methods, this work provides a picture of the adsorption ranging from the molecular to macroscopic levels.

Agreement between adhesion data and adsorption results confirm that there is greater interaction between anastellin and PU than between anastellin and PMMA. There appears to be agreement between the circular dichroism data and the molecular dynamics simulations of anastellin which both indicate a stable secondary structure. Molecular dynamics simulations of anastellin on polyurethane show that adsorption is strong and occurs rapidly. The simulations also show that the secondary structure of anastellin is stable upon adsorption to polyurethane in water and remains mostly stable even in saline solutions. Analysis of the simulations suggest that adsorption onto polyurethane is mediated by hydrophilic amino acids, due to hydrogen bonding with C=O and N-H groups in the polymer backbone, and residues in flexible regions of the protein.

17

Journal of Biomedical Materials Research Part A

to AFM and contact angle measurements was provided by the EPSRC Centre in Continuous

Manufacturing and Crystallisation (CMAC).

Journal of Biomedical Materials Research Part A

References

1. Vanterpool FA, Cantini M, Seib FP, Salmeron-Sanchez M. A material-based platform to modulate fibronectin activity and focal adhesion assembly. Biores Open Access 2014;3(6):286-96.

2. To WS, Midwood KS. Plasma and cellular fibronectin: distinct and independent functions during tissue repair. Fibrogenesis & Tissue Repair 2011;4(1):1-17.

3. Aota S, Nomizu M, Yamada KM. The short amino-acid-sequence Pro-His-Ser-Arg-Asn in human fibronectin enhances cell-adhesive function. Journal of Biological Chemistry 1994;269(40):24756-24761.

4. Agarwal R, González-García C, Torstrick B, Guldberg RE, Salmerón-Sánchez M, García AJ. Simple coating with fibronectin fragment enhances stainless steel screw osseointegration in healthy and osteoporotic rats. Biomaterials 2015;63:137-145.

5. Herranz-Diez C, Mas-Moruno C, Neubauer S, Kessler H, Gil FJ, Pegueroles M, Manero JM, Guillem-Marti J. Tuning mesenchymal stem cell response onto titanium-niobium-hafnium alloy by recombinant fibronectin fragments. ACS Appl Mater Interfaces 2016.

6. Petrie TA, Capadona JR, Reyes CD, Garcia AJ. Integrin specificity and enhanced cellular activities associated with surfaces presenting a recombinant fibronectin fragment compared to RGD supports. Biomaterials 2006;27(31):5459-70.

7. Hersel U, Dahmen C, Kessler H. RGD modified polymers: biomaterials for stimulated cell adhesion and beyond. Biomaterials 2003;24(24):4385-4415.

8. Morla A, Ruoslahti E. A fibronectin self-assembly site involved in fibronectin matrix assembly: reconstruction in a synthetic peptide. J Cell Biol 1992;118.

9. Yi M, Ruoslahti E. A fibronectin fragment inhibits tumor growth, angiogenesis, and metastasis. Proc Natl Acad Sci U S A 2001;98(2):620-4.

10. Morla A, Zhang Z, Ruoslahti E. Superfibronectin is a functionally distinct form of fibronectin. Nature 1994;367:193-6.

11. Kelsh R, You R, Horzempa C, Zheng M, McKeown-Longo PJ. Regulation of the innate immune response by fibronectin: synergism between the III-1 and EDA domains. PLoS One 2014;9(7):e102974.

12. Stine JM, Sun Y, Armstrong G, Bowler BE, Briknarova K. Structure and unfolding of the third type III domain from human fibronectin. Biochemistry 2015;54(44):6724-33.

13. Morla A, Ruoslahti E. A fibronectin self-assembly site involved in fibronectin matrix assembly: reconstruction in a synthetic peptide. J Cell Biol 1992;118(2):421-9.

14. Ohashi T, Erickson H. Domain unfolding plays a role in superfibronectin formation. Journal of Biological Chemistry 2005;280(47):39143-51.

15. Zheng M, Jones DM, Horzempa C, Prasad A, McKeown-Longo PJ. The First Type III Domain of Fibronectin is Associated with the Expression of Cytokines within the Lung Tumor Microenvironment. J Cancer 2011;2:478-83.

16. Ambesi A, Klein M, Pumiglia K, McKeown-Longo P. Anastellin, a fragment of the first type III repeat of fibronectin, inhibits extracellular signal-regulated kinase and causes G1 arrest in human microvessel endothelial cells. Cancer Research 2005;65:148-56.

17. Ambesi A, McKeown-Longo PJ. Anastellin, the angiostatic fibronectin peptide, is a selective inhibitor of lysophospholipid signaling. Mol Cancer Res 2009;7(2):255-65.

18. You R, Zheng M, McKeown-Longo PJ. The first type III repeat in fibronectin activates an inflammatory pathway in dermal fibroblasts. J Biol Chem 2010;285(47):36255-9.

19

Journal of Biomedical Materials Research Part A

19. Kowalczynska H, Nowak-Wyrzykowska M, Kolos R, Dobkowski J, Kaminski J. Fibronectin adsorption and arrangement on copolymer surfaces and their significance in cell adhesion. Journal of Biomedical Materials Research Part A 2005;72A(2):228-36.

20. Baugh L, Vogel V. Structural changes of fibronectin adsorbed to model surfaces probed by fluorescence resonance energy transfer. Journal of Biomedical Materials Research Part A 2004;69A(3):525-34.

21. Michael K, Vernekar V, Keselowsky B, Meredith J, Latour R, Garcia A. Adsorption-induced conformational changes in fibronectin due to interactions with well-defined surface chemistries. Langmuir 2003;19(19):8033-40.

22. Thevenot P, Hu W, Tang L. Surface chemistry influences implant biocompatibility. Curr Top Med Chem 2008;8(4):270-80.

23. Roach P, Farrar D, Perry CC. Interpretation of protein adsorption: Surface-induced conformational changes. Journal of the American Chemical Society 2005;127(22):8168-8173.

24. Krammer A, Lu H, Isralewitz B, Schulten K, Vogel V. Forced unfolding of the fibronectin type III module reveals a tensile molecular recognition switch. Proceedings of the National Academy of Sciences of the United States of America 1999;96(4):1351-1356.

25. Kowalczynska HM, Kolos R, Nowak-Wyrzykowska M, Dobkowski J, Elbaum D, Szczepankiewicz A, Kaminski J. Atomic force microscopy evidence for conformational changes of fibronectin adsorbed on unmodified and sulfonated polystyrene surfaces. Journal of Biomedical Materials Research Part A 2009;91A(4):1239-1251.

26. Lange D, Chew BH. Update on ureteral stent technology. Ther Adv Urol 2009;1(3):143-8.

27. Webb JCJ, Spencer RF. The role of polymethylmethacrylate bone cement in modern orthopaedic surgery. Journal of Bone & Joint Surgery, British Volume 2007;89-B(7):851-857.

28. Cassady AI, Hidzir NM, Grøndahl L. Enhancing expanded poly(tetrafluoroethylene) (ePTFE) for biomaterials applications. Journal of Applied Polymer Science 2014;131(15).

29. Palacio M, Schricker S, Bhushan B. Bioadhesion of various proteins on random, diblock and triblock copolymer surfaces and the effect of pH conditions. Journal of the Royal Society Interface 2011;8(58):630-40.

30. Palacio M, Schricker S, Bhushan B. Protein conformation changes on block copolymer surfaces detected by antibody-functionalized atomic force microscope tips. Journal of Biomedical Materials Research Part A 2012;100A(1):18-25.

31. Szott LM, Horbett TA. Protein interactions with surfaces: cellular responses, complement activation, and newer methods. Current Opinion in Chemical Biology 2011;15(5):677-682.

32. Raffaini G, Ganazzoli F. Molecular dynamics simulation of the adsorption of a fibronectin module on a graphite surface. Langmuir 2004;20(8):3371-8.

33. Panos M, Sen TZ, Ahunbay MG. Molecular simulation of fibronectin adsorption onto polyurethane surfaces. Langmuir 2012;28(34):12619-12628.

34. Kubiak-Ossowska K, Mulheran P, Nowak W. Fibronectin module FNIII9 adsorption at contrasting model surfaces studied by atomistic molecular dynamics. Journal of Physical Chemistry B 2014;118(33):9900-8.

35. Mallinson D, Alexiou P, Mullen A, Pelecanou M, Sagnou M, Lamprou DA. Isatin thiosemicarbazone-blended polymer films for biomedical applications: surface

20

Journal of Biomedical Materials Research Part A

morphology, characterisation and preliminary biological assessment. RSC Advances 2016.

36. Lamprou D, Smith J, Nevell T, Barbu E, Willis C, Tsibouklis J. Towards the determination of surface energy at the nanoscale: a further assessment of the AFM-based approach. Journal of Advanced Microscopy Research 2010;5:137-42.

37. Good R, van Oss C. The modern theory of contact angles and the hydrogen bond components of surface energies. In: G SMaL, editor. Modern Approach to Wettability: Theory and Applications. New York: Plenum; 1992.

38. Couston R, Lamprou D, Uddin S, van der Walle C. Interaction and destabilization of a monoclonal antibody and albumin to surfaces of varying functionality and hydrophobicity. International Journal of Pharmaceutics 2012;438:71-80.

39. Sugawara Y, Ohta M, Konishi T, Morita S, Suzuki M, Enomoto Y. Effects of humidity and tip radius on the adhesive force measured with atomic force microscopy. Wear 1993;168(1–2):13-16.

40. Rodahl M, Hook F, Kasemo B. QCM operation in liquids: An explanation of measured variations in frequency and Q factor with liquid conductivity. Analytical Chemistry 1996;68(13):2219-2227.

41. Kanazawa KK, Gordon JG. The oscillation frequency of a quartz resonator in contact with a liquid. Analytica Chimica Acta 1985;175(SEP):99-105.

42. Schumacher R, Borges G, Kanazawa KK. The quartz microbalance - a sensitive tool to probe surface reconstructions on gold electrodes in liquid. Surface Science 1985;163(1):L621-L626.

43. Hayakawa T, Yoshinari M, Nemoto K. Characterization and protein-adsorption behavior of deposited organic thin film onto titanium by plasma polymerization with hexamethyldisiloxane. Biomaterials 2004;25(1):119-127.

44. Hook F, Voros J, Rodahl M, Kurrat R, Boni P, Ramsden JJ, Textor M, Spencer ND, Tengvall P, Gold J and others. A comparative study of protein adsorption on titanium oxide surfaces using in situ ellipsometry, optical waveguide lightmode spectroscopy, and quartz crystal microbalance/dissipation. Colloids and Surfaces B-Biointerfaces 2002;24(2):155-170.

45. Wagberg L, Pettersson G, Notley S. Adsorption of bilayers and multilayers of cationic and anionic co-polymers of acrylamide on silicon oxide. Journal of Colloid and Interface Science 2004;274(2):480-488.

46. Tammelin T, Merta J, Johansson LS, Stenius P. Viscoelastic properties of cationic starch adsorbed on quartz studied by QCM-D. Langmuir 2004;20(25):10900-10909.

47. Wolff O, Seydel E, Johannsmann D. Viscoelastic properties of thin films studied with quartz crystal resonators. Faraday Discussions 1997;107:91-104.

48. Nigar M, Blackwell J, Chvalun SN, Seneker SD, Schmelzer HG. The structure of the hard domains in trans,trans-HMDI-based polyurethane elastomers. Acta Polymerica 1996;47(1):48-54.

49. MacKerell AD, Bashford D, Bellott M, Dunbrack RL, Evanseck JD, Field MJ, Fischer S, Gao J, Guo H, Ha S and others. All-atom empirical potential for molecular modeling and dynamics studies of proteins. J Phys Chem B 1998;102(18):3586-616.

50. Vanommeslaeghe K, Hatcher E, Acharya C, Kundu S, Zhong S, Shim J, Darian E, Guvench O, Lopes P, Vorobyov I and others. CHARMM general force field: A force field for drug-like molecules compatible with the CHARMM all-atom additive biological force fields. Journal of Computational Chemistry 2010;31(4):671-690.

51. Bussi G, Donadio D, Parrinello M. Canonical sampling through velocity rescaling. The Journal of Chemical Physics 2007;126(1):014101.

Journal of Biomedical Materials Research Part A

52. Hess B. P-LINCS: A parallel linear constraint solver for molecular simulation. Journal of Chemical Theory and Computation 2008;4(1):116-122.

53. Miyamoto S, Kollman PA. Settle: An analytical version of the SHAKE and RATTLE algorithm for rigid water models. Journal of Computational Chemistry 1992;13(8):952-962.

54. Essmann U, Perera L, Berkowitz ML, Darden T, Lee H, Pedersen LG. A smooth particle mesh Ewald method. The Journal of Chemical Physics 1995;103(19):8577-8593.

55. Hess B, Kutzner C, van der Spoel D, Lindahl E. GROMACS 4: Algorithms for highly efficient, load-balanced, and scalable molecular simulation. Journal of Chemical Theory and Computation 2008;4(3):435-447.

56. Dann JR. Forces involved in the adhesive process. Journal of Colloid and Interface Science 1970;32(2):321-331.

57. Elter P, Lange R, Beck U. Atomic force microscopy studies of the influence of convex and concave nanostructures on the adsorption of fibronectin. Colloids and Surfaces B Biointerfaces 2012;89:139-46.

58. Greenfield NJ. Using circular dichroism spectra to estimate protein secondary structure. Nat Protoc 2006;1(6):2876-90.

59. Briknarova K, Akerman M, Hoyt D, Ruoslahti E, Ely K. Anastellin, an FN3 fragment with fibronectin polymerization activity, resembles amyloid fibril precursors. Journal of Molecular Biology 2003;332:205-15.

60. Levy Y, Onuchic JN, Wolynes PG. Fly-casting in protein-DNA binding: frustration between protein folding and electrostatics facilitates target recognition. J Am Chem Soc 2007;129(4):738-9.

61. Aissaoui N, Bergaoui L, Landoulsi J, Lambert J-F, Boujday S. Silane layers on silicon surfaces: mechanism of interaction, stability, and influence on protein adsorption. Langmuir 2012;28(1):656-665.

22

Journal of Biomedical Materials Research Part A

Figure captions

Fig. 1 Second axis graphs with frequency and mass.

Fig. 2 Circular dichroism (CD) spectrum of FnIII1c.

Fig. 3 Difference in adhesion force by surface between silanised probes (APTES) and protein-functionalised probes (anastellin). All differences are significant.

Fig. 4 Density of anastellin on SiO_2, PU and PMMA surfaces.

Fig. 5 Protein centre-of-mass position (top) and orientation (bottom) for no salt simulations. Simulations starting in the Arg-down, Arg-up, C-down, and N-down conformations are denoted by black, red, green, and blue lines respectively.

Fig. 6 Simulation snapshots showing adsorption of anastellin on to polyurethane surface. (a) Protein in Arg-down starting configuration at (left to right) t = 0 ns, 13 ns, 25 ns, 47 ns, 50 ns, and 100 ns. (b) Protein in Arg-up starting configuration at (left to right) t = 0 ns, 5 ns, 10 ns, 48 ns, 55 ns, and 100 ns. (c) Protein in N-down starting configuration at (left to right) t = 0 ns, 1 ns, 15 ns, 20 ns, 50 ns, and 100 ns. (d) Protein in C-down starting configuration at (left to right) t = 0 ns, 1 ns, 10 ns, 27.5 ns, 47 ns, and 100 ns. Residues involved in adsorption (see text) are highlighted.

Fig. 7 Residue centre-of-mass positions for protein starting in (top to bottom) Arg-down, Arg-up, C-down, and N-down conformations.

Fig. 8 (a) Secondary structure amounts for (top to bottom) Arg-down, Arg-up, C-down, and N-down starting conformations. Black, red, and green lines denote turn, beta-strand, and random coil respectively. (b) Secondary structure distributions for (top to bottom) Arg-down, Arg-up, C-down, and N-down starting conformations.**Error! Reference source not found.**

Journal of Biomedical Materials Research Part A

Table 1 Advancing contact angles of SW, PMMA and PU surfaces, n = 12.

Surface	Contact Angle (θ_A °)		
	DW	DIM	EG
SW	56.6 ± 1.3	42.2 ± 2.6	33.9 ± 6.5
PMMA	74.7 ± 3.8	40.7 ± 1.1	59.2 ± 2.5
PU	85.9 ± 12.2	42.1 ± 7.5	60.0 ± 1.6

Table 2 Surface energy components by CAG and surface roughness by AFM of SW, PMMA, and PU surfaces.

Surface	Surface energy (mJ m^{-2})				Roughness by AFM
	γ_s^{LW}	γ_s^+	γ_s^-	γ_s	Ra (nm)
SW	38.49	0.30	23.98	43.81	0.11 ± 0.01
PMMA	39.26	0.14	13.63	42.02	2.00 ± 0.11
PU	38.54	0.00	4.07	38.67	3.06 ± 0.25

Table 3 Residues in contact with surface

Conformation	Residues in Contact
Arg-down	K21, N23, Q64, E65, T67, R68, D70
Arg-up	P7, Y61
C-down	N21, V23
N-down	A6, P7, Q8, Q60, Y61, G62

24

Journal of Biomedical Materials Research Part A

Equations

Equation 1

$A = 4\pi RT$

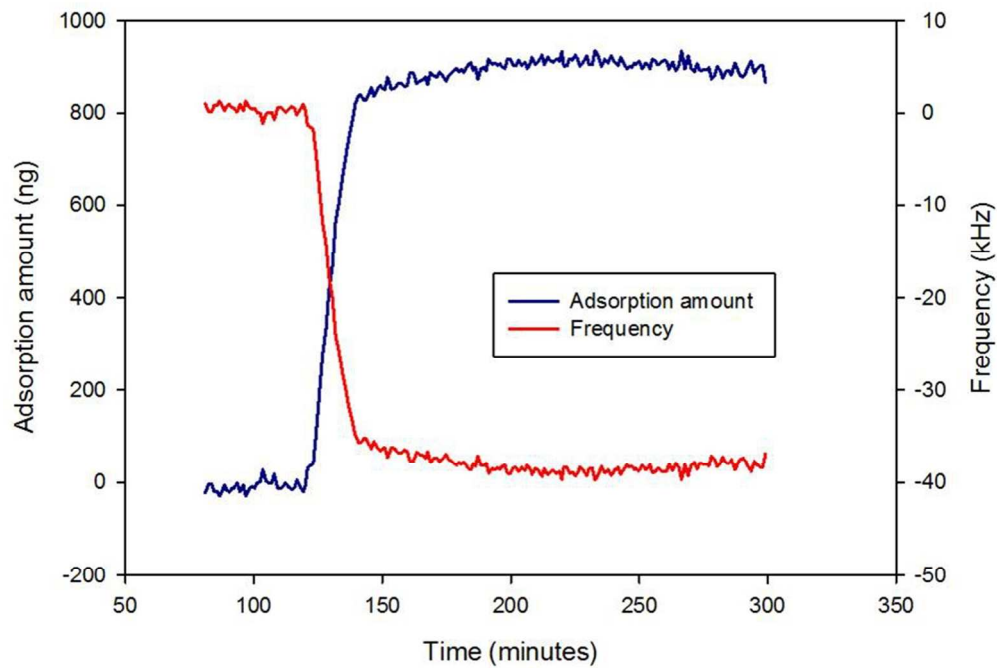Equation 2 Sauerbrey equation

$$\Delta m = \frac{C\,\Delta f n}{}$$

Fig. 1 Second axis graphs with frequency and mass.

218x161mm (111 x 111 DPI)
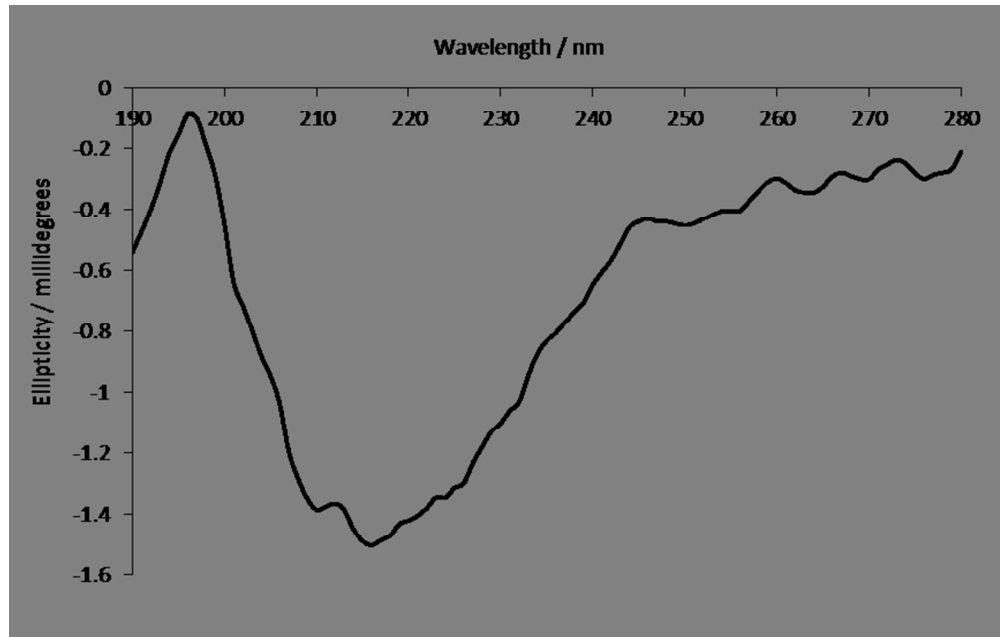
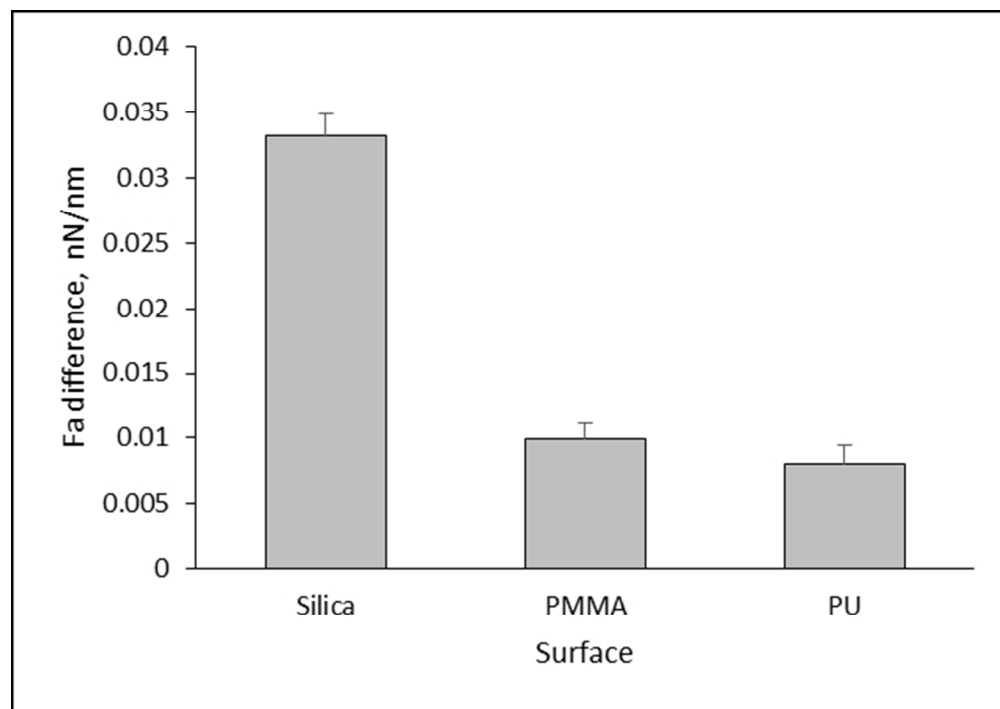Fig. 2 Circular dichroism (CD) spectrum of FnIII1c.

Fig. 3 Difference in adhesion force by surface between silanised probes (APTES) and protein-functionalised probes (anastellin). All differences are significant.
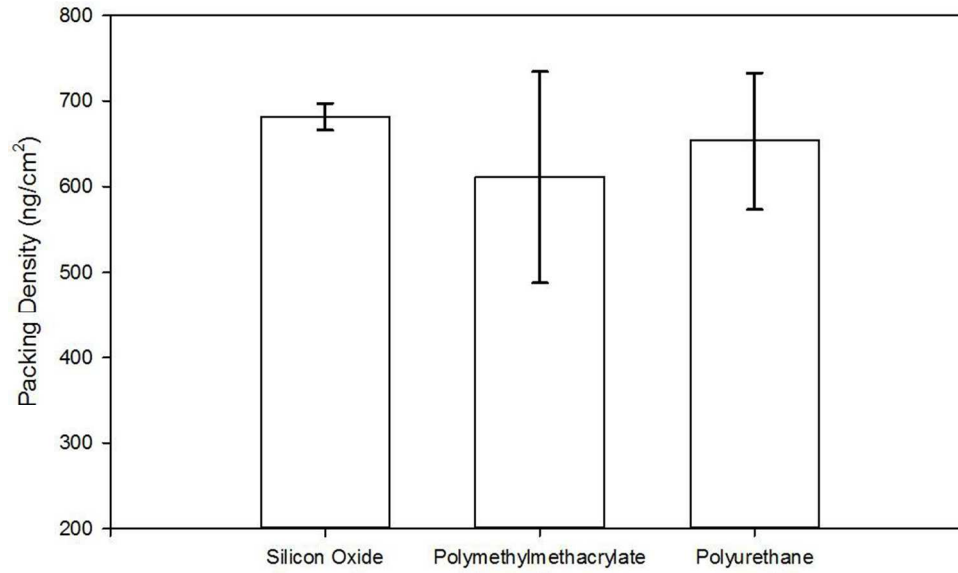
1
2
3
4
5
6
7
8
9
10
11
12
13
14
15
16
17
18
19
20
21
22
23
24
25
26
27
28
29
30
31
32
33
34
35
36
37
38
39
40
41
42
43
44
45
46
47
48
49
50
51
52
53
54
55
56
57
58
59
60

Fig. 4 Adsorbed mass of anastellin on SiO2, PU and PMMA surfaces.

174x113mm (150 x 150 DPI)
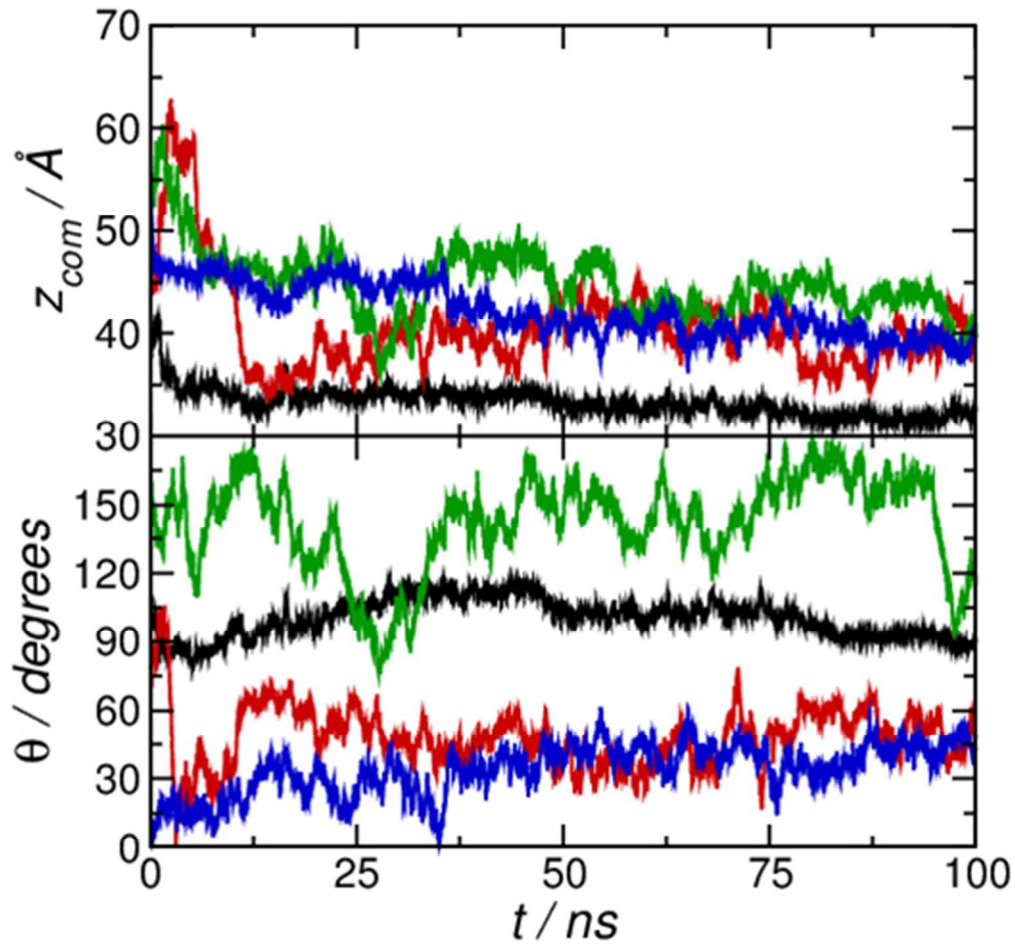
Fig. 5 Protein centre-of-mass position (top) and orientation (bottom) for no salt simulations. Simulations starting in the Arg-down, Arg-up, C-down, and N-down conformations are denoted by black, red, green, and blue lines respectively.
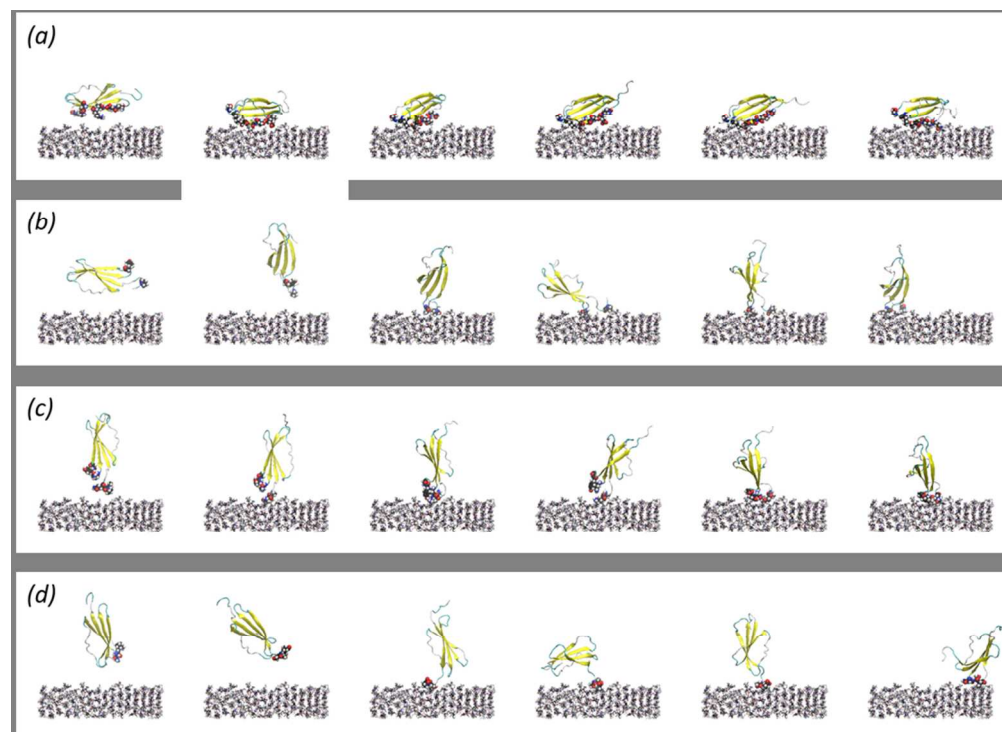
Fig. 6 Simulation snapshots showing adsorption of anastellin into polyurethane surface. (a) Protein in Arg-down starting configuration at (left to right) t = 0 ns, 13 ns, 25 ns, 47 ns, 50 ns, and 100 ns. (b) Protein in Arg-up starting configuration at (left to right) t = 0 ns, 5 ns, 10 ns, 48 ns, 55 ns, and 100 ns. (c) Protein in N-down starting configuration at (left to right) t = 0 ns, 1 ns, 15 ns, 20 ns, 50 ns, and 100 ns. (d) Protein in C-down starting configuration at (left to right) t = 0 ns, 1 ns, 10 ns, 27.5 ns, 47 ns, and 100 ns. Residues involved in adsorption (see text) are highlighted.
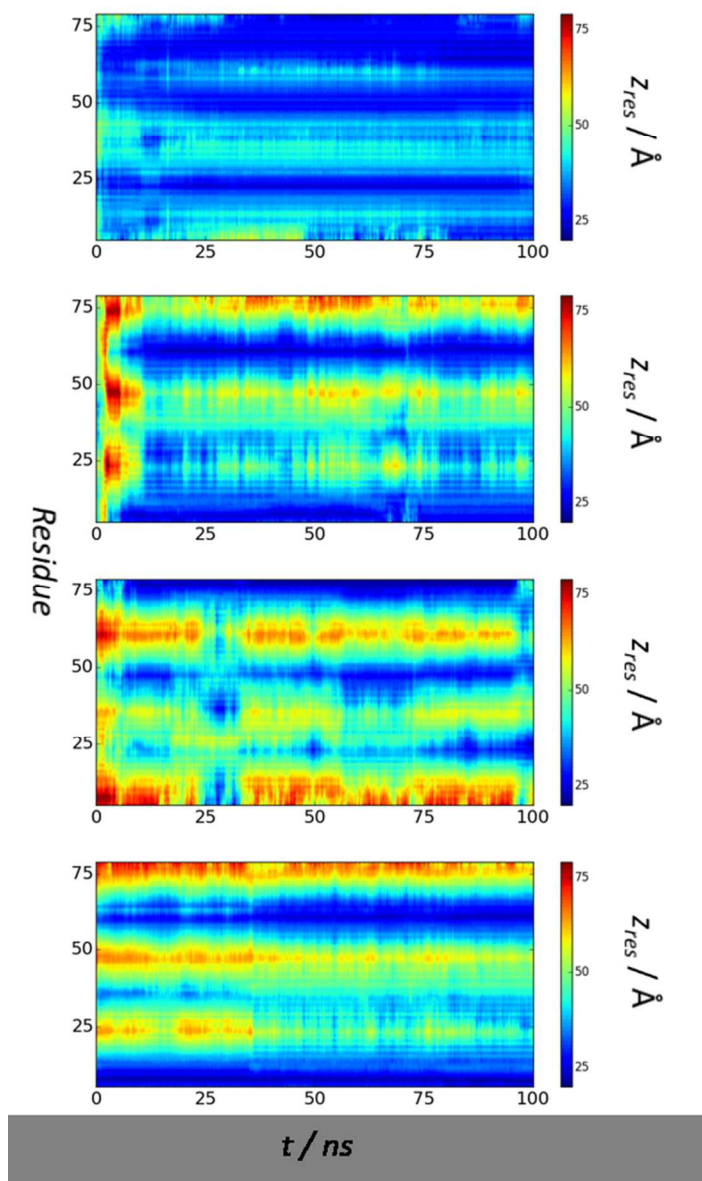
Fig. 7 Residue centre-of-mass positions for protein starting in (top to bottom) Arg-down, Arg-up, C-down, and N-down conformations.
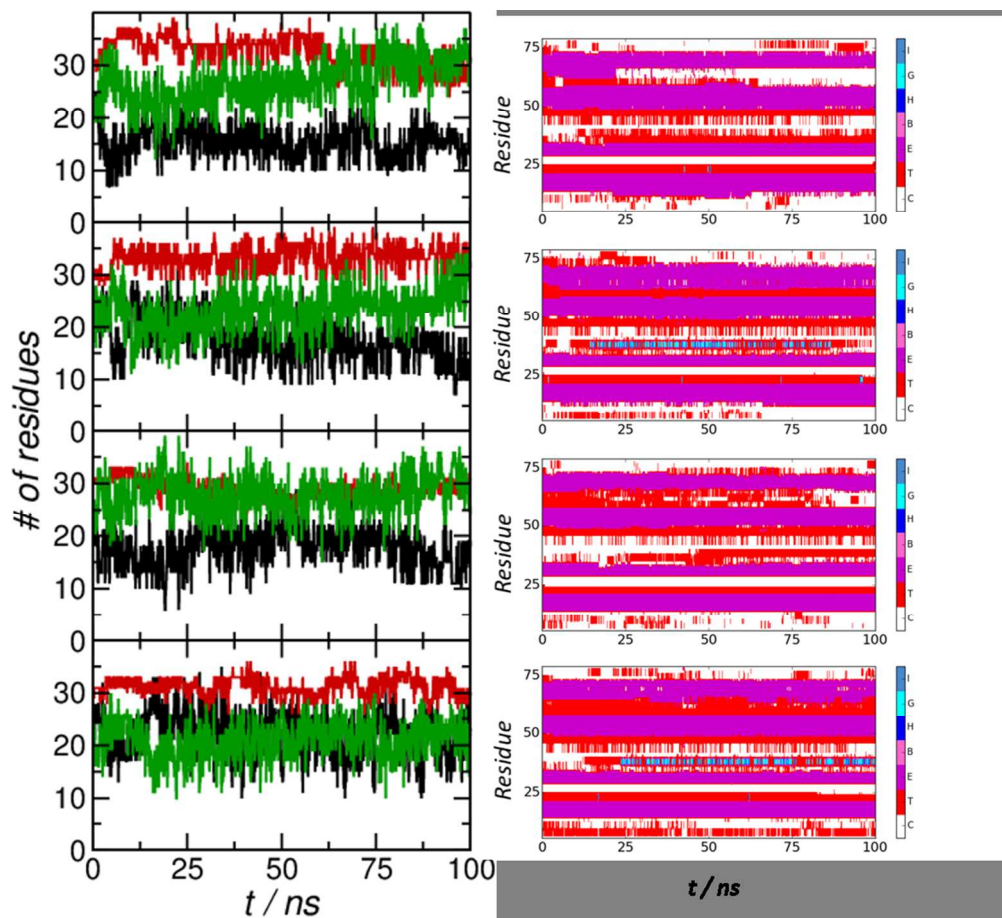
Fig. 8 (a) Secondary structure amounts for (top to bottom) Arg-down, Arg-up, C-down, and N-down starting conformations. Black, red, and green lines denote turn, beta-strand, and random coil respectively. (b) Secondary structure distributions for (top to bottom) Arg-down, Arg-up, C-down, and N-down starting conformations.